2007

Dynamics of small dust clouds trapped in a magnetized anodic plasma

Iris Pilch

Alexander Piel

Thomas Trottenberg

Mark E. Koepke

Dynamics of small dust clouds trapped in a magnetized anodic plasma

Iris Pilch,[a] Alexander Piel, and Thomas Trottenberg
Institut für Experimentelle und Angewandte Physik, Christian-Albrechts-Universität, D-24098 Kiel, Germany

Mark E. Koepke
Department of Physics, West Virginia University, Morgantown, West Virginia 26505-6315, USA

(Received 2 October 2007; accepted 8 November 2007; published online 10 December 2007)

Small dust clouds, which are confined in an anodic plasma, are studied with respect to their structure and their response to modulation of the anode bias. The dust cloud is displaced from the center of the discharge by a process similar to the void mechanism in radio-frequency discharges under microgravity. The top layers of the dust cloud are in a crystalline state and the cloud performs a slow rotation about the magnetic field direction. For modulation frequencies below 15 Hz, a sloshing and stretching motion in the confining potential well is found. Spontaneously excited dust density waves are observed when the dust cloud exceeds a minimum size. The waves are characterized by sickle-shaped wave fronts. No standing waves were found. The wave dispersion shows an influence of the boundedness of the system in terms of a frequency cutoff. © *2007 American Institute of Physics*. [DOI: 10.1063/1.2819315]

I. INTRODUCTION

Dust acoustic waves[1] are very-low-frequency density waves in a dusty plasma which involve the inertia of the dust particles and their shielded interaction force. The first observation of a dust acoustic-like wave was made by Thompson *et al.*[2] as a self-excited mode in a dust cloud trapped in an anodic plasma. The wave was excited by the ion current through the dust cloud and the waves propagated in the direction of the ion flow. Thompson *et al.* measured the dispersion relation of the wave by modulating the anode bias and found an almost acoustic dispersion of the density wave, as expected from the dust acoustic wave model.[1] Other authors studied a dust-acoustic instability in an inductive plasma,[3] the quenching of the unstable dust acoustic wave in a dc glow discharge by collisions,[4,5] or the spatial wave growth by particle-image-velocimetry.[6]

More recent investigations of this phenomenon by Trottenberg *et al.*[7] were focused on the confinement of the dust in the anodic plasma and on a refined analysis of the wave dispersion by comparing with a kinetic model.[8] The classical dust acoustic wave assumes an environment of thermal electrons and ions. Since the self-excited wave in experiments is driven by an ion drift, we prefer to call the waves in this more general situation dust density waves. Very recently, it was found that, in unmagnetized plasmas, dust density waves tend to propagate at an oblique angle to the ion drift when the ion drift speed exceeds the ion thermal speed.[9]

A central question in studying dust density waves is the influence of the system size on the wave propagation. Up to now, the analysis of experimental data was based on the comparison with theories that assume plane waves in an infinite homogeneous medium.[2,4,7] The role of boundaries, that act like a waveguide, on the dispersion of the wave were theoretically discussed with respect to a frequency cutoff.[10–12]

Small confined dust clouds that are embedded in a magnetized plasma and interact with an ion flow are interesting. They have internal structure that, in some ways, is similar and, in other ways, different from Yukawa balls.[13,14]

In the present paper we describe a detailed study of the dynamical behavior of such small dust clouds with respect to their structure, confinement, and internal density waves. The paper is organized as follows. The experimental arrangement is described in Sec. II and the shape and structure of the dust cloud is presented in Sec. III. The dynamics is studied at low modulation frequencies in terms of a "sloshing" motion in Sec. IV and at higher modulation frequencies as wave motion in Sec. V. The different observations are separately checked for consistency in Sec. VII.

II. EXPERIMENTAL SETUP

Figure 1(a) shows a longitudinal section of the plasma chamber. The cylindrical vacuum vessel has 104 cm length and 27 cm inner diameter. Ten magnetic field coils generate a homogenous magnetic field of typically 20 mT in the direction shown. A radio-frequency discharge at $f=27.12$ MHz is generated between a plane powered electrode (E) of 10 cm diameter and a plane grounded grid (G) at a distance of 5 cm, which are positioned at the right end of the device. This primary plasma source is operated at low power (1 W). The plasma expands through the grid and fills a column of 10 cm diameter which extends over the entire length of the vessel. Plasma density or plasma potential can be measured as a function of radius and axial position with a cylindrical Langmuir probe and an emissive probe, respectively, each supported by a shaft having a dog-leg geometry (P).

Our experiments are performed in argon gas at $p=3$ Pa. The plasma has a typical density of $n_e=10^{15}$ m^{-3}, an electron

[a]Electronic mail: pilch@physik.uni-kiel.de.

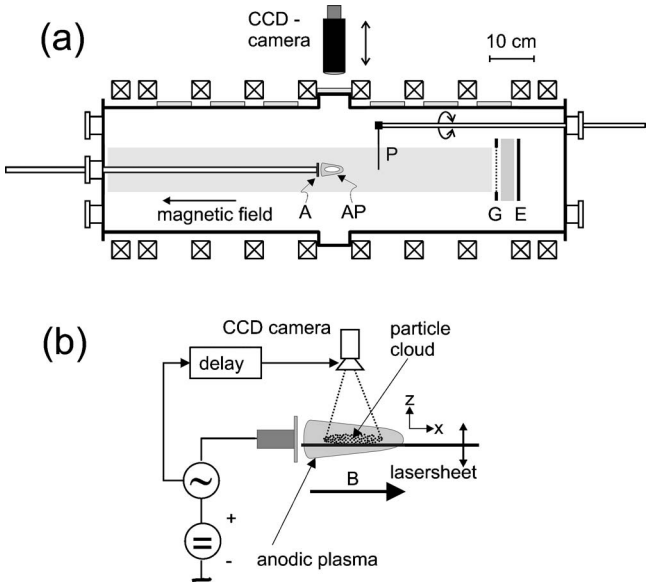

FIG. 1. (a) Cross section of the MATILDA II plasma device. (b) A dust cloud is trapped in the anodic plasma and observed with a combination of horizontal laser fan and camera. For stroboscopic recordings the camera shutter can be triggered from the signal generator.

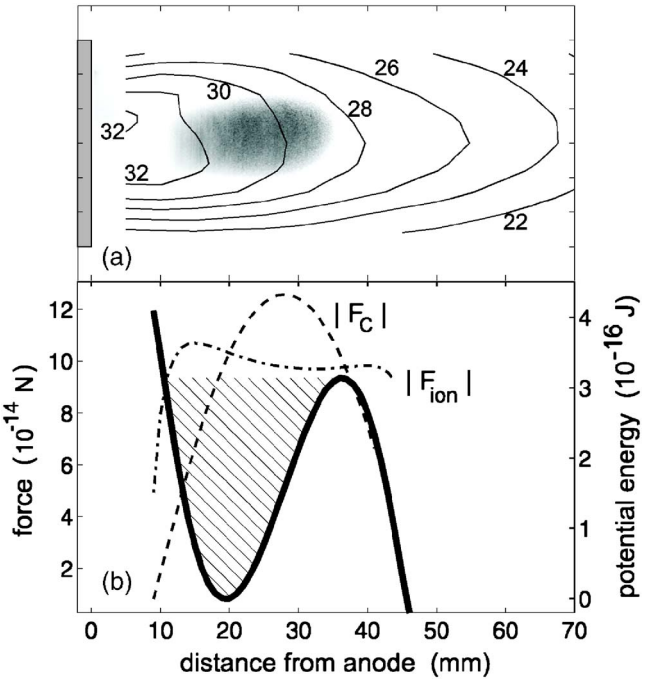

FIG. 2. (Color online) Axial confinement of a dust cloud in the anodic plasma (Ref. 7). (a) Contours of electric potential and top view of the dust cloud. (b) An effective potential well is formed by the electric force F_C and the ion drag force F_{ion}.

temperature of $T_e=3$ eV, and an ion temperature of $T_i=0.1$ eV.[7] We use spherical monodisperse dust particles (melamine formaldehyde) of 0.97 ± 0.05 μm diameter.

A secondary plasma is generated by biasing to high voltage $60\text{ V}\leqslant U_a\leqslant 75\text{ V}$ a small disk electrode (A) of 3 cm diameter, which is inserted axially. This phenomenon is known from low-pressure arcs[15] and was used as a plasma contactor.[16] At high values of currents drawn by the disk, a "fireball" is formed which takes the shape of a cylinder, i.e., a "firerod," in the presence of a magnetic field.[17] In the following we refer to the disk as "anode" and call this secondary plasma "anodic plasma." The formation of such an anodic plasma is also found in other experiments on dust acoustic waves with confined dust.[2,18,19]

Dust lying on a small tray below is spontaneously repelled from the tray and attracted into the anodic plasma above a certain anode bias voltage, here $U_a\approx 120$ V. The confinement of dust in front of the anode disk was studied in detail by Trottenberg *et al.*[7] The potential contours in Fig. 2(a), which is reproduced here for further reference, were obtained from measurements of the two-dimensional potential structure with an emissive probe. The dust is trapped in an effective potential well [see Fig. 2(b)], that is formed by an inhomogeneous axial electric field and the ion drag force. Radial confinement is made possible by a moderate magnetic field, which is responsible for an enhancement of the radial electric field compared to the axial electric field, which we understand to be the influence of the different Hall parameters of electrons and ions.

Coherent waves can be generated by Thompson's technique[2] of adding a sinusoidal modulation voltage to the anode bias. We use an ac voltage of $U_{\text{mod}}=10\text{ V}_{pp}$ superimposed on the dc voltage of $60\text{ V}\leqslant U_a\leqslant 75$ V. The observation geometry and image acquisition method for the structure and dynamics of small dust clouds are sketched in Fig. 1(b). The dust cloud is illuminated by a laser light sheet ($\lambda=532$ nm, 200 mW) and the scattered light is recorded by a camera which is placed above the experiment. The camera has a CCD sensor with 480×640 pixels and a frame rate of 150 fps at maximum resolution. Laser light sheet and camera with a macro lens are mounted on a translation stage and can be vertically positioned to image any horizontal plane of the plasma. In this way, the dust cloud can be scanned volumetrically in a series of horizontal slices.

Phase synchronous recording of the wave can be achieved by triggering the camera shutter from the square-wave output of the signal generator that delivers the modulation voltage. The shutter time of the camera is small (2 ms) with respect to the period of the modulation voltage. This kind of recording gives a stroboscopic image of the wave, which can be either used for averaging the image or for detecting any jitter about the average image. The phase between the trigger pulse and the camera shutter can be varied by a pulse delay unit. In a second mode of operation, the camera is triggered from a signal generator at $f=8\times f_{\text{mod}}$ that is phase-locked with the modulation generator. Such a high frame rate can be achieved by selecting a smaller region of interest.

In the following, we use a coordinate system in which the x-axis is aligned with the magnetic field direction, the y-axis is in the horizontal plane, and the z-axis defines the vertical direction. We will use the terminology of a "small" dust cloud when the dimensions are smaller than a typical wavelength of the dust density wave, $d<\lambda$. The cloud is called "medium" size for $2\lambda<d<3\lambda$ and "large" for $d\gg\lambda$.

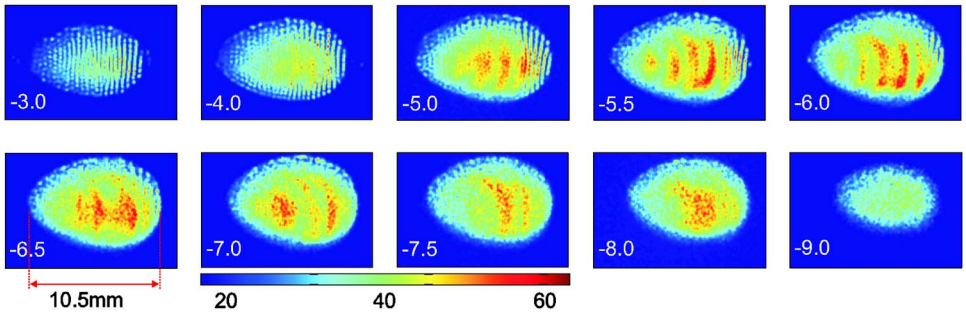

FIG. 3. (Color online) A series of horizontal sections of the dust cloud obtained by stroboscopic recording and averaging of 100 subsequent frames. The numbers refer to the z-position.

III. THE STRUCTURE OF THE DUST CLOUD

Small and medium sized dust clouds in the anodic plasma take the shape of a prolate ellipsoid, which are aligned with the magnetic field direction. A typical dust cloud of medium size is shown in Fig. 3 as a series of horizontal sections. Each image is generated with the stroboscopic technique and represents the average of 100 time-adjacent frames. The dust cloud has a length of 10.5 mm and a diameter of 7.3 mm. The numbers in each image indicate the vertical position of the section in millimeters with respect to the center of the anode disk. Obviously the dust cloud is horizontally centered with the anodic plasma but we note that it is shifted vertically (by 6 mm) to a lower position. The mean interparticle distance is $b=440\ \mu$m, which corresponds to a dust density $n_d \approx b^{-3}=1.2\times 10^{10}\ \mathrm{m}^{-3}$. The total number of particles in the dust cloud is $N_d \approx 3.8\times 10^4$.

Inspecting the images in Fig. 3, two features become immediately evident. First, there is a pronounced structure of parallel stripes in the sections between −3.0 mm and −6.0 mm, which become increasingly blurred at lower positions. The stripes have a distance of 450 μm, which corresponds to the typical interparticle distance. Second, there are curved wave fronts of a dust density wave visible in the sections between −5.0 mm and −8.0 mm. The wave pattern appears as alternating light and dark sickle-shaped wave fronts.

The stripes are oriented exactly perpendicular to the magnetic field. We interpret the equal spacing and alignment of the stripes as a crystalline ordering in the upper part of the dust cloud. The lower half of the cloud is in a liquid phase. The cloud performs a slow rotation about the magnetic field direction due to the azimuthal component of the ion motion, which exerts a torque on the dust cloud by ion drag. In view of the wave activity, we cannot perform a reliable three-dimensional structural analysis by means of scanning video microscopy, as it was done for Yukawa balls.[13]

However, we can analyze the intrinsic orientational order in each individual frame of the stroboscopic movie. A single frame of the movie corresponding to position $z=-3$ mm is shown in Fig. 4(a). In particular in the right half of the cloud, an intrinsic order can be seen that prefers alignment in a direction perpendicular to the magnetic field. This ordering can be quantified by a histogram of the bond-orientational order. For this purpose we define the bond angle of nearest neighbors (nn) $\theta_{ij}=\arctan[(x_i-x_j)/(y_i-y_j)]$ and a histogram function,

$$h(\theta)=\sum_{i=1}^{N}\sum_{j\in\{\mathrm{nn}\}}\delta(\theta-\theta_{ij}). \tag{1}$$

We define a nearest neighbor as particle having a distance of less than 1.3 b, when b is the mean interparticle distance. At last, the histogram is averaged over 1024 frames and normalized to unity. The polar plot of this histogram in Fig. 4(b) shows a sharp peak in the $\pm y$-direction which indicates the alignment perpendicular to the magnetic field direction. The

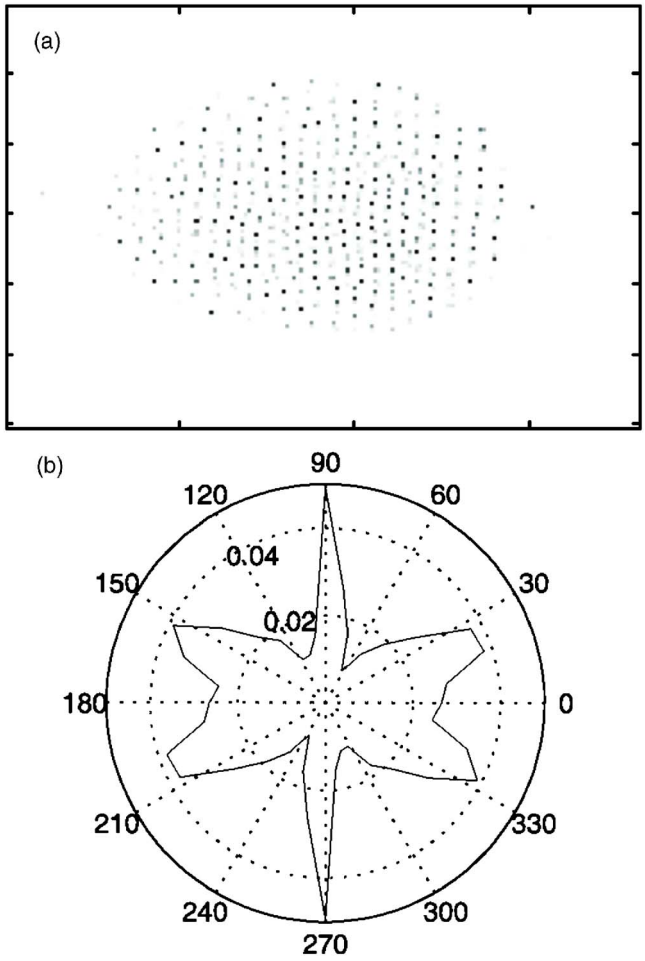

FIG. 4. (Color online) (a) The arrangement of the dust particles in a single frame (corresponding to $z=-3.0$ mm in Fig. 3) hints at a preference to form aligned ordering perpendicular to the magnetic field. (b) Polar plot of the bond-order histogram observed in individual frames, averaged over 100 frames. The sharp peaks at 90°/270° confirm the alignment. The pattern can be interpreted as the superposition of a sixfold and fourfold symmetry.

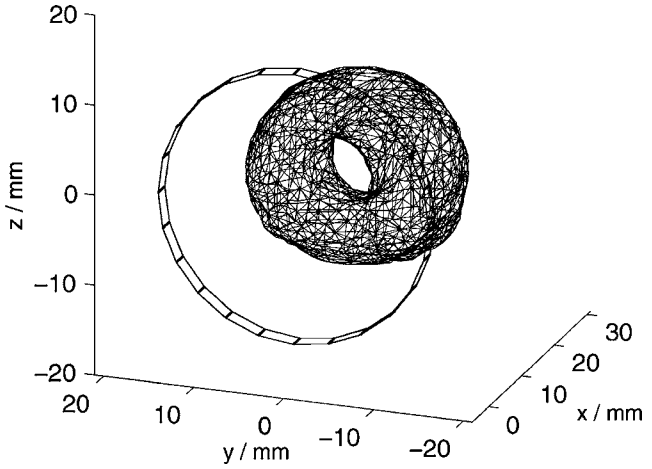

FIG. 5. Equidensity contour of the scattered light from a dust cloud of submicron particles. The central hole of this toroidal shape is interpreted as a void region, in which the ion drag force exceeds the radial electric field force.

polar plot has six pronounced lobes. This indicates a preference for a sixfold symmetry. However, the maxima of the broader lobes form angles of more than 60° with respect to the aligned peaks and the minima between the broader peaks are less deep than the minima adjacent to the sharp peaks. This finding is a hint at the admixture of a fourfold symmetry.

Careful inspection of the dust density distribution in a horizontal section of the cloud (see, e.g., Fig. 3 at $z=-4$ mm) shows a dark gap close to the boundary of the dust cloud which contains no particles. Such a gap was also observed in experiments with large Yukawa balls,[13] which tend to be in a liquid state, and was interpreted as an induced radial order at the surface caused by the strong force gradient of the confinement.

At higher magnetic field (50 mT) and gas pressure (5 Pa), large dust clouds can attain the topology of a torus with a central hole. The shape of the cloud is reconstructed here by measuring the intensity distribution of scattered light in a sequence of vertically displaced slices and calculating three-dimensional contour surfaces. Such an equidensity contour is shown in Fig. 5. This torus is slowly rotating in the $\vec{j}_i \times \vec{B}$ direction. Torus formation requires a sufficient amount of dust in the system and an azimuthal component of the ion drag force that is able to lift the dust against gravity.

IV. SLOSHING MOTION

The dynamical response of a dust cloud of small or medium size to a modulation of the anode bias depends on the applied frequency. For modulation frequencies 1 Hz$\leqslant f_{\mathrm{mod}} \leqslant$15 Hz, these clouds perform a periodic axial motion, which we call "sloshing." For medium-sized clouds, self-excited internal density waves are found, which can be synchronized by the external modulation force at higher frequencies of 20 Hz$\leqslant f_{\mathrm{mod}} \leqslant$40 Hz.

An example for the response of a small dust cloud at different phases during modulation at $f_{\mathrm{mod}}=4$ Hz is shown in Fig. 6. The dc bias was $U_a=70$ V and the modulation voltage

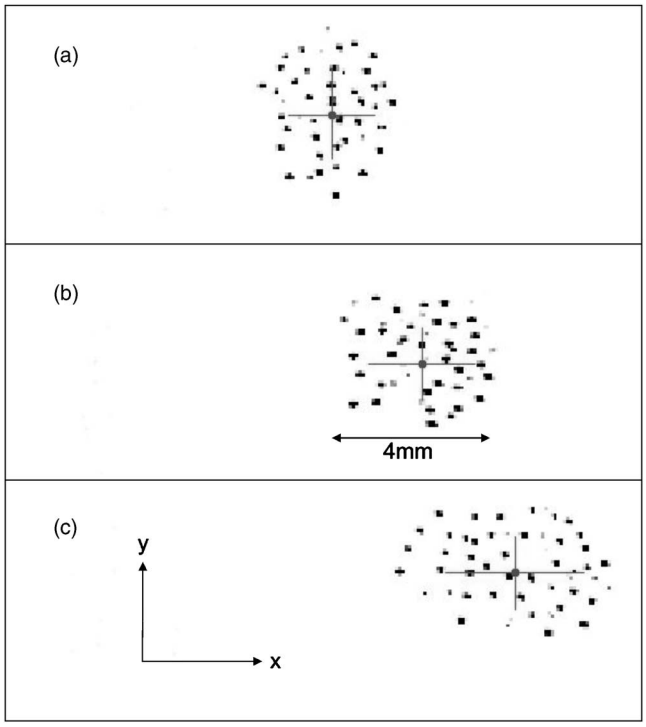

FIG. 6. Inverted-intensity image of the dust cloud in different phases of the motion. (a) Left turning point of the motion, (b) equilibrium position, (c) right turning point. The c.o.m. position x_{com} and the deformations d_x, d_y are indicated with bars.

$U_{\mathrm{mod}}=10\ \mathrm{V}_{pp}$. We find that the dust particles in this small cloud are not crystallized but perform a fast irregular motion. The figure shows the shape of the dust cloud (a) at the left turning point, (b) at the equilibrium position, and (c) at the right turning point. It becomes evident that the cloud is axially compressed in panel (a) whereas it is stretched in panel (c). Hence we can distinguish two different effects: The cloud performs a periodic center-of-mass motion along the x-direction, which is aligned with the magnetic field. Simultaneously, the cloud experiences a quadrupole-like deformation, which, however, is only seen in a cross section. The two processes can be quantified by studying the center-of-mass (c.o.m.) coordinate of the dust cloud, which we can estimate from the center of scattered light intensity in a movie frame. Let $B_{i,j}$ be the brightness of a pixel at coordinates (x_i, x_j). Then the center of mass becomes

$$x_{\mathrm{com}}(t) = \frac{1}{B_{\mathrm{tot}}(t)} \sum_{i=0}^{N-1} \sum_{j=0}^{M-1} x_j B_{ij}(t), \tag{2}$$

where $B_{\mathrm{tot}}(t)=\Sigma_i \Sigma_j B_{ij}(t)$ is the total intensity in that frame and x_j is the x-coordinate corresponding to pixel index j. Likewise, the stretching of the dust cloud is obtained by calculating the second moment of the intensity distribution

$$d_x^2 = \frac{1}{B_{\mathrm{tot}}(t)} \sum_{i=0}^{N-1} \sum_{j=0}^{M-1} [x_j - x_{\mathrm{com}}(t)]^2 B_{ij}(t). \tag{3}$$

The sloshing amplitude in the x-direction is dependent on the applied frequency (full circles) in Fig. 7. The c.o.m. motion at the lowest frequency ($f_{\mathrm{mod}}=1$ Hz) is representative for the

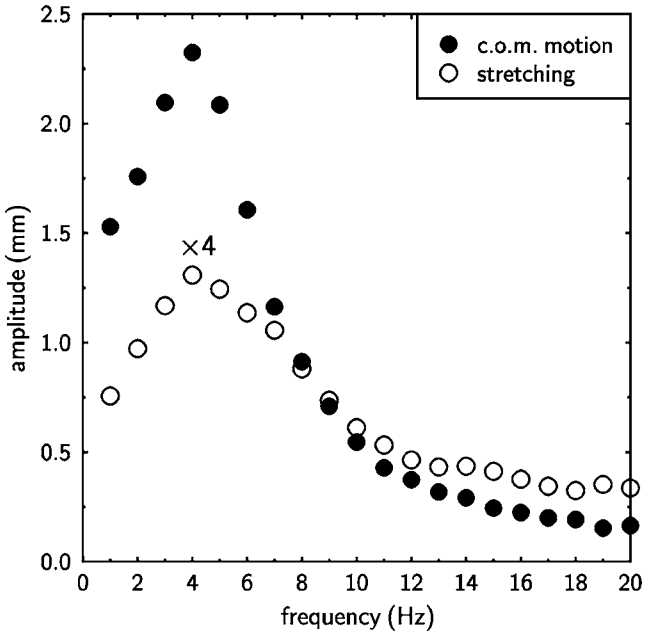

FIG. 7. Sloshing amplitude and stretching amplitude of a small dust cloud as a function of modulation frequency. Both amplitudes show a resonance maximum at 4 Hz.

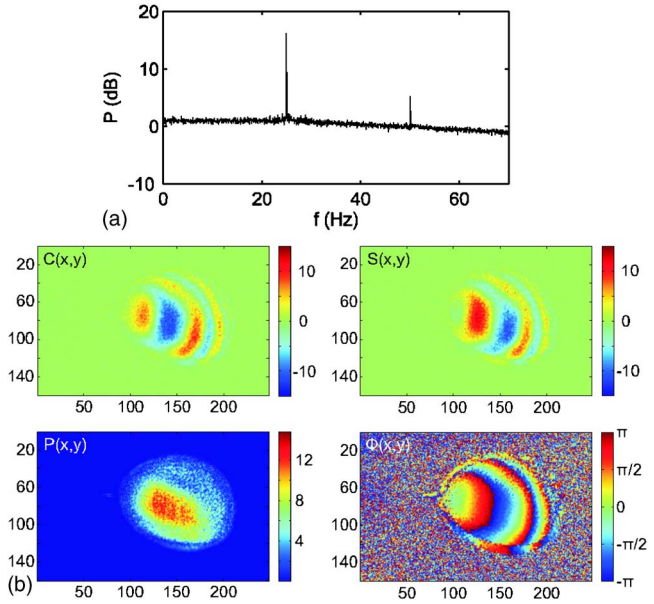

FIG. 8. (Color online) (a) Average spectral power density of the fluctuations of scattered light in a central square of 21×21 pixels. (b) Reconstructed wave function in terms of real part $C(x,y)$ and imaginary part $S(x,y)$ as well as intensity distribution $P(x,y)$ and phase $\phi(x,y)$.

static shift of the dust cloud's equilibrium position with applied anode bias U_a. With increasing frequency, the sloshing amplitude becomes larger and attains a maximum at 4 Hz. For even larger frequencies, the sloshing amplitude decreases slightly more rapidly with increasing frequency. Obviously, the sloshing motion has a resonant response to the external modulation. A similar behavior with a resonance at the same frequency is found for the stretching of the dust cloud (circles in Fig. 7). A periodic motion of the c.o.m. and a quadrupole deformation is also observed in medium sized dust clouds, however, with a lower amplitude than for small clouds.

V. THE PHASE FRONTS OF DUST DENSITY WAVES

Here, we analyze the phase evolution of a dust density wave in the central horizontal section of the dust cloud. We can make use of the wave information contained in a long movie consisting of F frames by observing that the spectral power density has a dominant sharp peak at the frequency f_{mod} and has an additional peak at its harmonic $2f_{\mathrm{mod}}$, which together represent the coherent wave motion, see Fig. 8(a).

For the determination of the phase fronts from a given movie, the brightness distribution in each frame $B_k(x,y)$ of the movie at time t_k is projected on the fundamental modes $\sin(2\pi f_{\mathrm{mod}}t)$ and $\cos(2\pi f_{\mathrm{mod}}t)$. The smaller contribution of the second harmonic is presently neglected. In this way, we obtain the complex spatial wave function $C(x,y)+\mathrm{i}S(x,y)$,

$$S(x,y)=\sum_{k=1}^{F} B_k(x,y)\sin(2\pi f_{\mathrm{mod}}t_k), \tag{4}$$

$$C(x,y)=\sum_{k=1}^{F} B_k(x,y)\cos(2\pi f_{\mathrm{mod}}t_k). \tag{5}$$

From the complex wave function we deduce the phase distribution $\phi(x,y)$ and the wave intensity $P(x,y)$,

$$\phi(x,y)=\arctan\left(\frac{S(x,y)}{C(x,y)}\right), \tag{6}$$

$$P(x,y)=\sqrt{S(x,y)^2+C(x,y)^2}. \tag{7}$$

These four functions are compiled in Fig. 8(b), which was recorded with the eightfold supersampling technique. The complex wave function confirms the result of the stroboscopic measurement in Fig. 3 that the wave fronts are curved. This curvature and the origin of the wave from a spot on the left-hand side of the dust cloud become even more evident in the phase distribution. The wave amplitude decreases towards the edge of the dust cloud.

Because the individual slices have a fixed phase relationship we can deduce the shape of the phase fronts in a vertical section through the center of the dust cloud from a sequence of horizontal sections. In Fig. 9 the resulting wave function is shown as real and imaginary part. For comparison, the shape of the dust cloud is indicated by the dotted boundary line. The wave fronts are inclined and show that the wave propagation has both an axial and a downwards component. This orientation is compatible with the assumed ion flow direction which has the same pattern.

VI. WAVE DISPERSION

The dispersion of the density wave is estimated from the apparent wavelength λ^* measured in a horizontal section of the dust cloud. The true wavelength λ corresponds to the perpendicular distance between two wave fronts as seen in Fig. 9 and $\lambda=\lambda^*\cos\alpha$, where α is the inclination of the propagation vector $\vec{k}$ with respect to the horizontal. We use

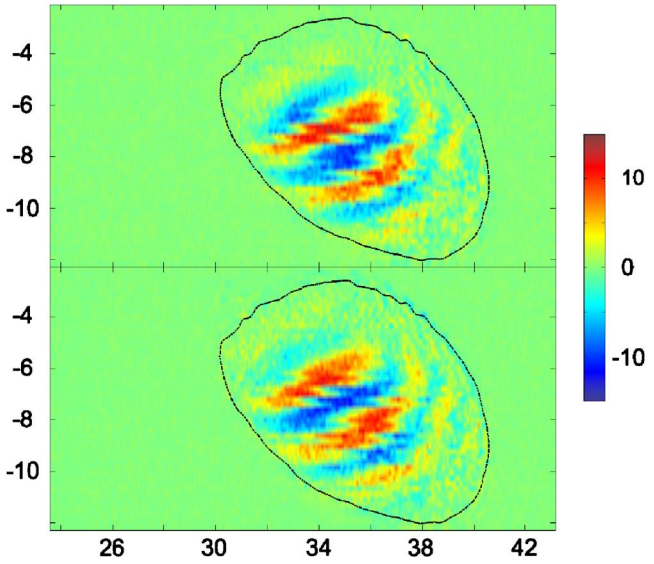

FIG. 9. (Color online) The reconstructed real (top) and imaginary part (bottom) of the wave function in a vertical section of the dust cloud. The labels give the x and z coordinates (in mm) with respect to the center of the anode disk. The boundary of the dust cloud is marked by the dotted line.

an estimate of $\alpha \approx 45°$ in the following. This measured wavelength λ^* varies with the modulation frequency f_{mod} as shown in Fig. 10.

For comparison, we have plotted the long wavelength limit of the dust acoustic wave dispersion, $\omega = \omega_{pd} \lambda_D k$, and the cylindrical-waveguide mode of Shukla and Rosenberg,[10] which, when dust neutral collisions are neglected, is given by

$$\omega = \omega_{pd} \left[\frac{k^2 + \gamma^2}{k_D^2 + k^2 + \gamma^2} \right]^{1/2}. \tag{8}$$

Here, $k_D = 1/\lambda_D$ and $\gamma = 2.4/R$ represents the fundamental mode. This gives (at $k=0$) a cutoff frequency $\omega_{\mathrm{min}} = \omega_{pd}\, \gamma (k_D^2 + \gamma^2)^{-1/2}$. At our experimental conditions ($n_d = 1.7 \times 10^{10}$ m^{-3}, $Z_d = 3000$) we obtain $\omega_{pd} \approx 780$ s^{-1}. The diameter $2R \approx 5$ mm of the waveguide is estimated from the transverse dimension of the dust cloud in Fig. 9.

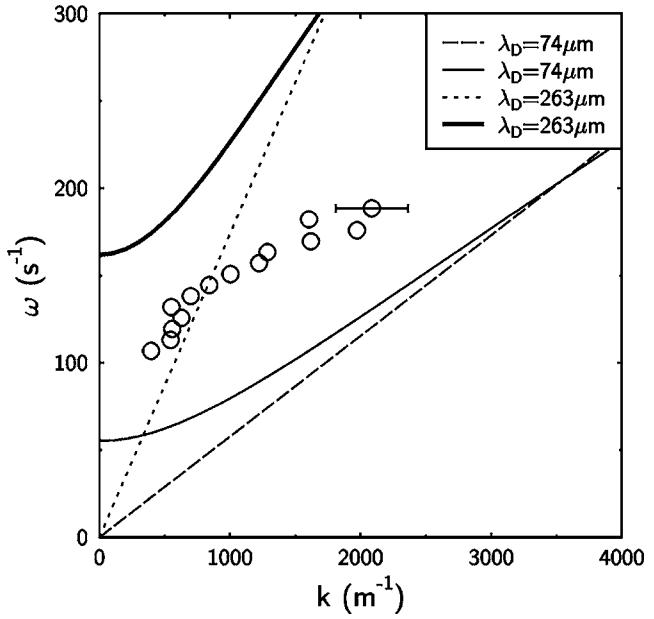

FIG. 10. Measured dispersion in the center of a small dust cloud in comparison with the acoustic dispersion of a dust acoustic wave (dashed and dotted line) and the fundamental waveguide mode from Ref. 10 (full lines).

For the waveguide mode we consider two limiting cases. In the first case, assuming thermal ions with $k_B T_i = 0.1$ eV, the ion Debye length becomes $\lambda_{Di} = 74$ μm and, because $T_e \gg T_i$, $\lambda_D \approx \lambda_{Di}$. Then the dust acoustic velocity becomes 74 mm/s, which is smaller than the observed phase velocities. In the second case, we assume that the ions have the Bohm speed, $v_B = \omega_{pi} \lambda_{D,e}$. In this limit, ion shielding is reduced and the estimated ion shielding length is $\lambda_{D,i} \approx \lambda_{D,e}$, which results in $\lambda_D \approx 2^{-1/2} \lambda_{D,e}$.

The data points lie between both limiting cases and show that, in the experiment, the group velocity is smaller than the phase velocity. This effect is different from a dust acoustic wave, which has identical group and phase velocity in the long-wavelength limit. Such a difference, however, is found in the waveguide modes as a consequence of the frequency cutoff.

VII. DISCUSSION

A. Confinement

The small dust clouds were found vertically displaced from the axis of the anodic plasma. One could imagine that the levitation might be described by the balance of weight force and electric field force, $m_d g = Z_d e E_r$. For the known electric field $E_r \approx 10^3$ V m^{-1}, however, the dust charge estimate becomes $Z_d = 48$ only, which is unreasonably small. The model for axial confinement[7] required $Z_d \approx 2000-3000$ instead. Hence, the radial confinement is also determined by a balance of ion drag force and electric field force. This means that the observed radial displacement from the center of the anodic plasma is equivalent to the formation of a dust-free void[20] in the center, as observed in rf discharges under microgravity.[21] The force balance at the void edge was recently quantified experimentally.[22]

For slightly different plasma parameters and using a large amount of dust, we have found a toroidal shape of the dust cloud with a central hole. This is an immediate hint at the formation of a central void region. In an earlier investigation[7] we had shown that the critical electric field for void formation, at our present plasma parameters, has the value of ≈ 180 V m^{-1}. Comparing the potential contours in Fig. 2, this is a realistic value expected at the position $z = -3$ mm, where the force equilibrium for the top side of the spheroidal cloud is established.

B. Structure

The formation of stripes on the topside of a small dust cloud can be understood by crystallization in the top layer and slow rotation of the cloud about the magnetic field direction. The observed pattern is different from the nested shell structure found in Yukawa balls.[13] The assumed dust charge $Z_d = 3000$ is sufficiently large that the Coulomb coupling parameter $\Gamma = (Z_d e)^2 / (4\pi\epsilon_0 a_{\mathrm{WS}} k_B T_d)$ attains a large value $\Gamma = 1900$. Here, $a_{\mathrm{WS}} = [3/(4\pi n_d)]^{1/3}$ is the Wigner-Seitz

radius, which becomes $a_{WS}=271\ \mu m$ at $n_d=1.2\times10^{10}\ m^{-3}$. For comparison, the critical values for melting in an extended system with Yukawa interaction with a shielding factor $\kappa=a_{WS}/\lambda_D$ are $\Gamma_{crit}=172,217,440,1185,\ldots$ for $\kappa=0,1,2,3,\ldots$.[23] Therefore, the parameters in our system allow crystallization provided that $\kappa\leqslant3$ and that the dust is at room temperature.

Rotational motion of dust clouds in a magnetic field is attributed to the azimuthal component of the ion motion that exerts a weak torque on the dust cloud. For our experimental conditions, the ion Hall parameter takes a value of $\omega_{ci}/\nu_{in}\approx0.1$, which means that the ion velocity is preferentially oriented in the electric field direction and has a smaller azimuthal component, which is 10% of that velocity. Although the torque is weak, the damping rate of the rotational motion by dust-neutral friction is also small and allows a constant rotation. The orientation of the electric field direction can be estimated from Fig. 2(a). At a distance of $x=36$ mm from the anode and $z=-8$ mm, which corresponds to the center of the dust cloud in Fig. 9, the electric field has an inclination of 60°–80° from the horizontal. This compares fairly well with the inclination of the wavevector in Fig. 9.

The fact that the top layers of the dust cloud are crystalline while the lower layers are found in a liquid state may be explained by the excitation of the dust density wave. This wave attains large amplitudes in the center of the cloud, which results in particle displacements that exceed the Lindeman melting criterion.[24] Because the ion streaming direction has both an axial and a downward component, it is not surprising that the top layer, where the wave has small amplitude, can remain crystalline while the growing wave amplitude leads to the melting down to the bottom of the cloud.

C. Sloshing and stretching

The observed sloshing motion attains a resonant enhancement at a frequency of 4 Hz. For comparison, the eigenfrequency determined by the curvature of the effective potential well shown in Fig. 2(b) at its lowest point is 12.6 Hz. This difference can be explained by assuming a weaker curvature of the confining well at the position of the small dust cloud.

The observed stretching of the dust cloud cannot be explained by the periodic motion in a strictly parabolic confining potential. In that case, the particle cloud would move like a rigid body. The typical confining well shown in Fig. 2(b), however, has an asymmetric shape with a pronounced "softening" that becomes visible as an inflection on the right-hand side. Hence, such an asymmetry, which we also expect for the confining well of the small dust cloud, allows for a stretching at the right turning point and a compression at the left turning point.

D. Phase fronts of dust density waves

Different from the observation in extended dust clouds,[2,7] where the approximation of nearly plane waves could be justified, the phase fronts in small dust clouds have a pronounced curvature. This was already seen in the stroboscopic image in Fig. 3 and becomes even more pronounced in the small dust cloud in Fig. 8. Apparently, the waves emerge from a spot at the left-hand side of the dust cloud and form a set of sickle-shaped regions that propagate to the right.

One could imagine that the wave fronts are determined by the eigenmodes of a small spheroidal cloud. Such eigenmodes are composed of forward and reflected waves. In the present case, the forward wave is an unstable wave that is fed by the streaming ions. In the observed plane the ions have an axial (parallel to x) and radial (parallel to $\pm y$) velocity. Therefore, all parts of the curved wave front can be considered as being amplified by the ion streaming motion. The opposite situation is found for any reflected wave, which propagates against the ion flow. Consequently, the reflected wave is damped with a damping length comparable to the wavelength. The damping of the reflected wave is therefore responsible for the nonestablishment of global standing waves.

We could extract the vertical structure of the wave fronts from a set of individual horizontal slices which were mutually phase synchronous. The wave fronts are asymmetric with respect to the dust cloud and describe a propagation direction that has an axial and a downward component. This orientation is consistent with the expected ion streaming direction.

E. Wave dispersion

We have found that because of the inclined wave propagation with respect to a horizontal section of the cloud, the apparent wavelength λ^* is longer than the true wavelength λ. Varying the wave frequency, we find a dispersion that deviates from the dust acoustic wave in an infinite medium. The group velocity is found smaller than the phase velocity. This behavior is found consistent with the waveguide mode,[10] and can be attributed to a frequency cut-off. A similar frequency cutoff was found for dust acoustic waves in a plasma slab,[12] which can be considered as a dielectric waveguide. Therefore, the influence of the finite transverse dimension of the dust cloud is insensitive to the kind of boundary condition (metallic/dielectric). Although the model of a cylindrical waveguide is only a rough approximation for a small dust cloud, the essential feature that results from a frequency cutoff is reproduced in our experiment.

F. Consistency of the observations

The crystallization of medium size dust clouds requires that $\kappa<3$. Therefore, the linearized Debye length must be $\lambda_D>150\ \mu m$. Such an increase beyond the thermal ion Debye length (74 μm) is expected when the ion drift speed comes close to the Bohm velocity. The ion mobility and the radial electric field at the position of confinement result in such a high speed. Hence, the structural properties of and the wave dispersion in medium size dust clouds can be described by a consistent set of plasma parameters.

The Schweigert instability[25,26] involves chain formation by wakefield attraction and excitation of short-wavelength transverse modes, which eventually lead to melting of plasma crystals. It was observed in unmagnetized plasmas

with multilayer dust systems in the sheath of radio-frequency discharges. This instability appears for ion drift speeds that exceed the Bohm speed. In the present experiments, the ion drift speed is close to the Bohm speed. Therefore, we cannot rule out that wakefield attraction is also acting here. In medium size dust clouds, the unstable dust density wave may mask the Schweigert instability. One could also speculate that a contribution from wakefield attraction favors the fourfold symmetry in parts of the crystallized top layers. In small dust clouds, the appearance of a fluid phase with high dust velocities may hint at the action of the Schweigert instability.

The large dust clouds studied in Ref. 7 are not affected by a vertical inclination of the wave front because these clouds were nearly centered with the anode disk. Therefore, a distinction between λ and λ^* was unnecessary. Moreover, the cross section of the cloud was larger by a factor of 2–3. Since the radius of the waveguide enters as $1/R^2$ in Eq. (8), the influence of the frequency cut-off becomes negligible and the interpretation of the wave dispersion in terms of a kinetic model is not affected by our new finding.

In summary, we present a first exhaustive survey of the structure and dynamical features of small and medium size dust clouds. Novel findings are the void formation in a dc discharge, the strict alignment of a crystal axis perpendicular to the magnetic field, and the competition of sixfold and fourfold symmetry. The full three-dimensional structure of the phase fronts of dust density waves reveals that the waves propagate in the direction of the local electric field.

ACKNOWLEDGMENTS

The present investigations were financially supported by DFG within the transregional collaborative research center TR-24, Project No. A2. M.E.K. acknowledges partial support by the U.S. NSF.

[1] N. N. Rao, P. K. Shukla, and M. Y. Yu, Planet. Space Sci. **38**, 543 (1990).
[2] C. Thompson, A. Barkan, N. D'Angelo, and R. L. Merlino, Phys. Plasmas **4**, 2331 (1997).
[3] A. V. Zobnin, A. D. Usachev, O. F. Petrov, and V. E. Fortov, JETP **95**, 429 (2002).
[4] S. Ratynskaia, M. Kretschmer, S. Khrapak, R. A. Quinn, M. H. Thoma, G. E. Morfill, A. Zobnin, A. Usachev, O. Petrov, and V. Fortov, IEEE Trans. Plasma Sci. **32**, 613 (2004).
[5] S. Ratynskaia, S. Khrapak, A. Zobnin, M. H. Thoma, M. Kretschmer, A. Usachev, V. Yaroshenko, R. A. Quinn, G. E. Morfill, O. Petrov, and V. Fortov, Phys. Rev. Lett. **93**, 085001 (2004).
[6] E. Thomas, Jr., Phys. Plasmas **13**, 042107 (2006).
[7] T. Trottenberg, D. Block, and A. Piel, Phys. Plasmas **13**, 042105 (2006).
[8] M. Rosenberg, J. Plasma Phys. **67**, 235 (2002).
[9] A. Piel, M. Klindworth, O. Arp, A. Melzer, and M. Wolter, Phys. Rev. Lett. **97**, 205009 (2006).
[10] P. K. Shukla and M. Rosenberg, Phys. Plasmas **6**, 1038 (1999).
[11] N. X. Wei and J. K. Xue, Phys. Plasmas **13**, 052101 (2006).
[12] V. Yaroshenko, H. Thomas, and G. Morfill, Phys. Plasmas **14**, 082104 (2007).
[13] O. Arp, D. Block, and A. Piel, Phys. Rev. Lett. **93**, 165004 (2004).
[14] O. Arp, D. Block, M. Klindworth, and A. Piel, Phys. Plasmas **12**, 122102 (2005).
[15] L. Malter, E. Johnson, and W. Webster, RCA Rev. **12**, 415 (1951).
[16] B. Song, N. D'Angelo, and R. Merlino, J. Phys. D **24**, 1789 (1991).
[17] T. An, R. Merlino, and N. D'Angelo, J. Phys. D **27**, 1906 (1994).
[18] E. Thomas and M. Watson, Phys. Plasmas **6**, 4111 (1999).
[19] E. Thomas, Phys. Plasmas **8**, 329 (2001).
[20] J. Goree, G. E. Morfill, V. N. Tsytovich, and S. V. Vladimirov, Phys. Rev. E **59**, 7055 (1999).
[21] G. E. Morfill, H. M. Thomas, U. Konopka, H. Rothermel, M. Zuzic, A. Ivlev, and J. Goree, Phys. Rev. Lett. **83**, 1598 (1999).
[22] M. Wolter, A. Melzer, O. Arp, M. Klindworth, and A. Piel, IEEE Trans. Plasma Sci. **35**, 266 (2007).
[23] S. Hamaguchi, R. Farouki, and D. H. E. Dubin, Phys. Rev. E **56**, 4671 (1997).
[24] J. P. Hansen and I. R. McDonald, *Theory of Simple Liquids*, 2nd ed. (Academic, London, 1990).
[25] A. Melzer, V. Schweigert, I. Schweigert, A. Homann, S. Peters, and A. Piel, Phys. Rev. E **54**, R46 (1996).
[26] V. A. Schweigert, I. V. Schweigert, A. Melzer, A. Homann, and A. Piel, Phys. Rev. E **54**, 4155 (1996).